# Regional Variations of Moist Static Energy Flux into the Arctic*

JAMES E. OVERLAND

*Pacific Marine Environmental Laboratory/NOAA, Seattle, Washington*

PHILIP TURET

*Joint Institute for the Study of Atmosphere and Ocean, University of Washington, Seattle, Washington*

ABRAHAM H. OORT

*Geophysical Fluid Dynamics Laboratory/NOAA, Princeton, New Jersey*

(Manuscript received 25 May 1994, in final form 7 March 1995)

ABSTRACT

The authors investigate the climatological heating of the Arctic by the atmospheric moist static energy (MSE) flux from lower latitudes based on 25 years (November 1964–1989) of the GFDL dataset. During the five month winter period (NDJFM) the transport of sensible heat by transient eddies is the largest component (50%) at 70°N, followed by the transport of sensible heat by standing eddies (25%), and the moist static energy flux by the mean meridional circulation (25%). The mean meridional circulation (MMC) changes from a Ferrel cell to a thermally direct circulation near 60°N; maximum horizontal velocities in the thermally direct circulation peak near 70°N. North of 60°N the sensible heat flux by the MMC is southward and opposes the greater northward transport of geopotential energy. The transport of energy is not uniform. Major pathways are the northward transport of positive anomalies through the Greenland and Barents Seas into the eastern Arctic and the southward transport of negative anomalies to the east of the Siberian high. The Atlantic pathway in winter relates to transport by transient eddies, while the western Siberian flux relates to the standing eddy pattern. Interannual variability of northward MSE is concentrated in these two regions. The western Arctic Ocean from about 30° to 60°W receives about 50 W $m^{-2}$ less energy flux convergence than the eastern Arctic. This result compares well with the observed minimum January surface air temperatures in the Canadian Basin of the western Arctic and implies that the greater observed ice thickness in this region may have a thermodynamic as well as a dynamic origin.

## 1. Introduction

The primary energy balance in the Arctic is between advection of moist static energy (MSE), that is, sensible heat, potential energy, and latent heat from lower latitudes, and net radiation of energy outward at the top of the atmosphere. These fluxes are positive in all seasons of the year as the Arctic provides the Northern Hemisphere sink for the atmospheric thermodynamic engine. In response to the large annual cycle in solar radiation received, the sea ice and upper ocean absorb heat energy during the summer season and are a net energy source during the long winter season.

The annual cycle of this energy flux across 70°N was estimated by Nakamura and Oort (1988, hereafter NO), who calculated outward radiation fluxes from satellite data and latitudinal fluxes from atmospheric rawinsonde observations over a ten-year period, 1963–1973. More recently Overland and Turet (1994, hereafter OT) extended the analyses to 25 years, 1965–1989. Results were similar between NO and OT. The northward flux across 70°N was equivalent to an energy flux convergence of 121 W $m^{-2}$ in winter (NDJFM) when normalized by the surface area north of 70°. This compares to a net radiation balance at the ice surface of 30 W $m^{-2}$ and a sensible heat flux of 10 W $m^{-2}$ (Maykut 1986; Overland and Guest 1991). The balance of the atmospheric heat is radiated to space. The summer MSE flux (JJA) across 70°N was equivalent to 85 W $m^{-2}$. Over the 25-year period the interannual standard deviation of MSE for the winter period was small, 11 W $m^{-2}$. This compares to the month to month variability of 34 W $m^{-2}$. Even though the winter interannual variability of MSE is relatively small, one might expect that it would force a larger variability of ice cover than is observed (Untersteiner 1990). Transport of sen-

* Pacific Marine Environmental Laboratory Contribution Number 1516. Joint Institute for Study of Atmosphere and Ocean Contribution Number 261.

*Corresponding author address:* Dr. James E. Overland, Pacific Marine Environmental Laboratory, NOAA, Building No 3, 7600 Sand Point Way, N.E., Seattle, WA 98115.

TABLE 1. Definition of variables and parameters.

| | |
|---|---|
| $C_p$ | Specific heat at constant pressure |
| $g$ | Gravity |
| $L$ | Latent heat of evaporation |
| $T$ | Temperature |
| $z$ | Geopotential height |
| $q$ | Specific humidity |
| $p$ | Pressure |
| $x$ | Unit distance (m) |
| $\lambda$ | Longitude |
| $t$ | Time |
| $\tau$ | Time-averaging interval |

sible heat by transient eddies was the largest contributor to the northward MSE flux at nearly 50%. Standing eddies and the mean meridional circulation each contributed about 25% to the northward flux in winter. Latent heat transport was not negligible, making up 7% of the total flux in winter and 20% in summer.

The surface energy budgets of 1D coupled sea ice–atmospheric models (i.e., a vertical column) that rep-

TABLE 2. Mean fluxes across 70°N for the annual, 3-month winter (DJF), 5-month winter (NDJFM), and 3-month summer (JJA) periods (after OT). Units are watts per square meter, representing the latitudinal flux divided by the surface area north of 70°N.

| | Annual | DJF | NDJFM | JJA |
|---|---|---|---|---|
| $F_{\text{wall}}$ | 103 | 121 | 121 | 85 |
| TE | 56 | 58 | 58 | 53 |
| SE | 22 | 35 | 33 | 11 |
| MMC | 25 | 27 | 31 | 20 |
| SH | 44 | 68 | 63 | 21 |
| TE | 45 | 52 | 51 | 35 |
| SE | 19 | 33 | 31 | 8 |
| MMC | −21 | −17 | −18 | −22 |
| GP | 48 | 44 | 49 | 47 |
| TE | −1 | −1 | −1 | 0 |
| SE | 0 | 0 | 0 | 0 |
| MMC | 48 | 45 | 50 | 48 |
| LH | 11 | 8 | 9 | 17 |
| TE | 12 | 7 | 8 | 18 |
| SE | 2 | 2 | 2 | 3 |
| MMC | −3 | −1 | −1 | −5 |

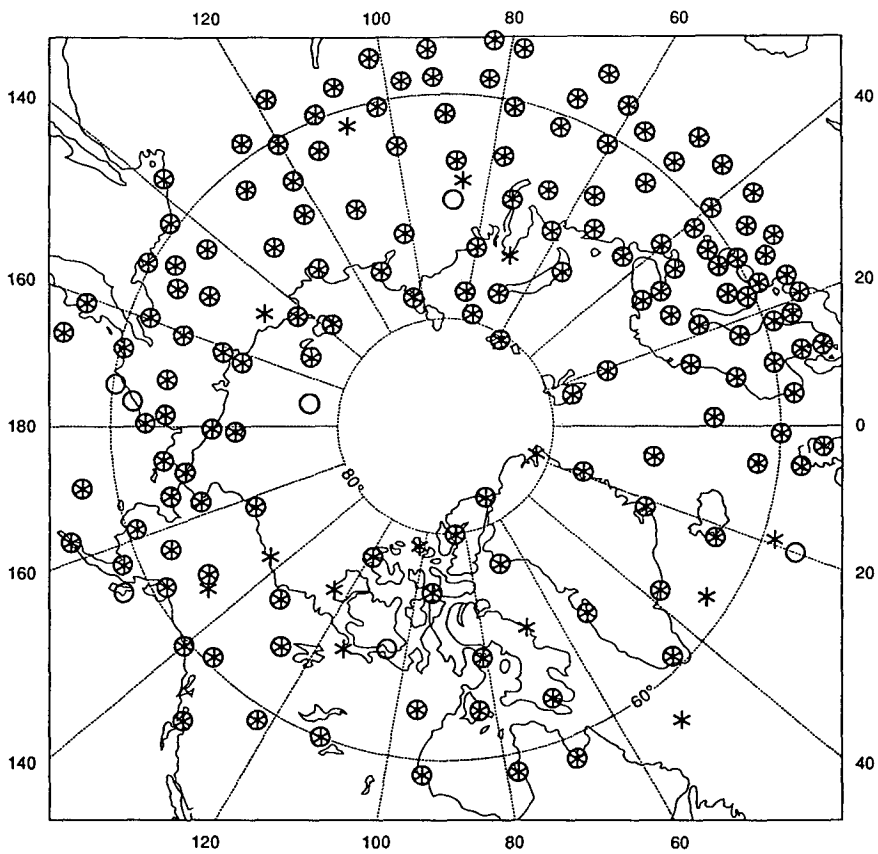


FIG. 1. Distribution of rawinsonde stations at 500 mb for the North Polar region for January 1969 (indicated by an asterisk) and January 1989 (indicated by a circle). Only those stations are shown that have 10 or more good daily reports of wind and temperature at 500 mb during the month. There were 161 stations north of 55°N in 1969, and 151 stations in 1989.

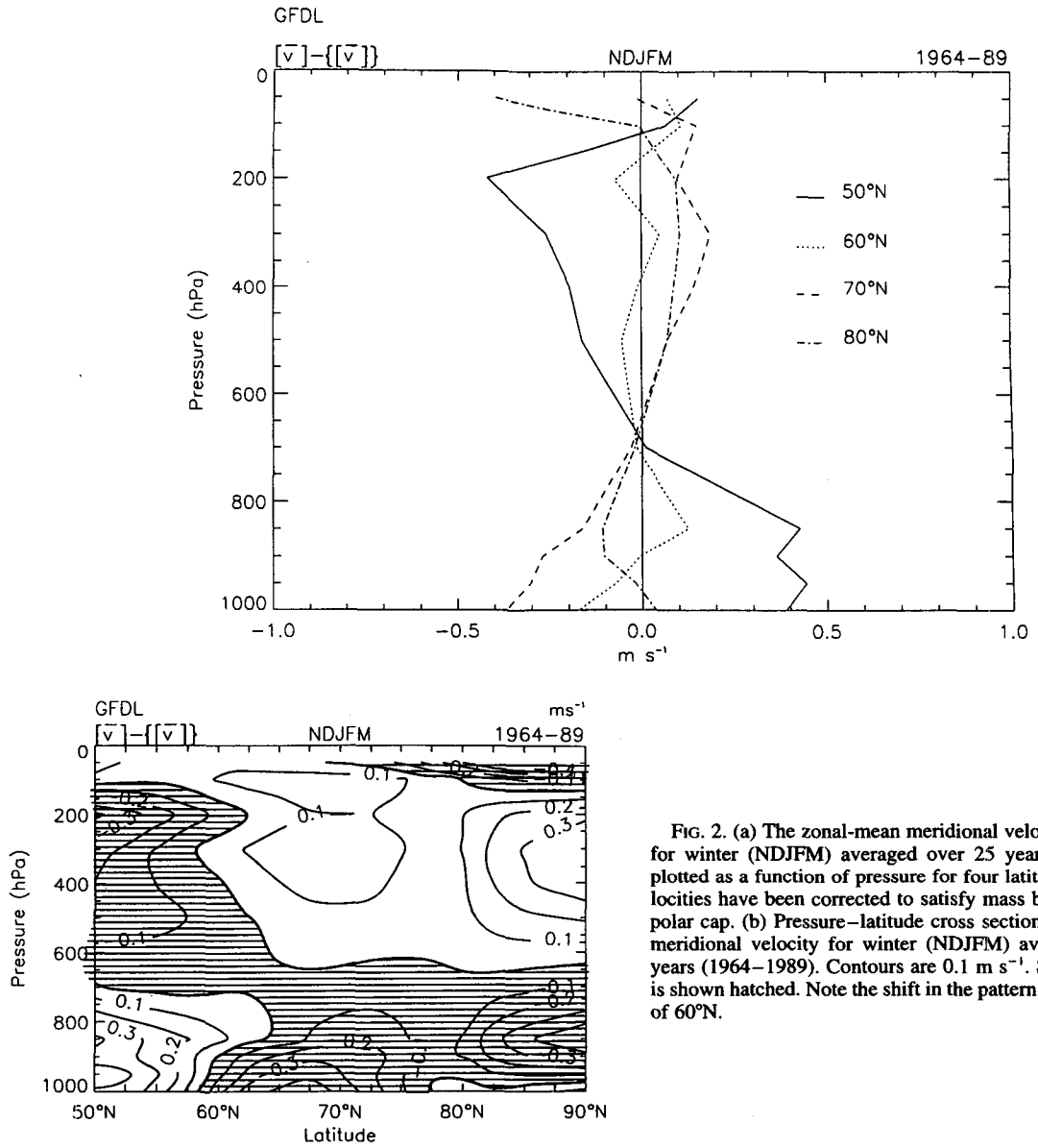


FIG. 2. (a) The zonal-mean meridional velocity component for winter (NDJFM) averaged over 25 years (1964–1989) plotted as a function of pressure for four latitude circles. Velocities have been corrected to satisfy mass balance over the polar cap. (b) Pressure–latitude cross section of zonal-mean meridional velocity for winter (NDJFM) averaged over 25 years (1964–1989). Contours are 0.1 m $s^{-1}$. Southward flow is shown hatched. Note the shift in the pattern north and south of 60°N.

resent the "central Arctic" (Overland and Guest 1991; Moritz et al. 1992) require an additional atmospheric heating from flux convergence of about 1°C $d^{-1}$, which fits well with the observed latitudinal energy flux across 70°N. Yet these models are very sensitive to the atmospheric horizontal energy flux values as shown by Thorndike's (1992) calculation in which a change in the northward flux of +30 W $m^{-2}$ above an annual value of 100 W $m^{-2}$ could result in an ice-free Arctic and a change of −20 W $m^{-2}$ could result in a permanent ice pack 12 m thick. Although Thorndike's model does not include all possible feedbacks, particularly cloud cover (Royer et al. 1990), it is highly suggestive of the sensitivity of a 1D heat balance to the horizontal flux convergence. The observed latitudinal energy flux appears to exhibit large longitudinal variations (OT) and, as we shall see, also large latitudinal variations. If a 1D coupled model is applied to a subregion of the Arctic where the flux convergence differs substantially from the mean, it may not produce a reasonable closed energy budget. This difference between regional and basinwide budgets produces a paradox. Does the horizontal transport of sea ice thickness redistribute, spatially as well as temporally, the energy that originated as atmospheric energy flux convergence and communicated to the sea ice through the radiation balance? The latter question is beyond the scope of the present paper. Here we wish to expand the analyses of the Geo-

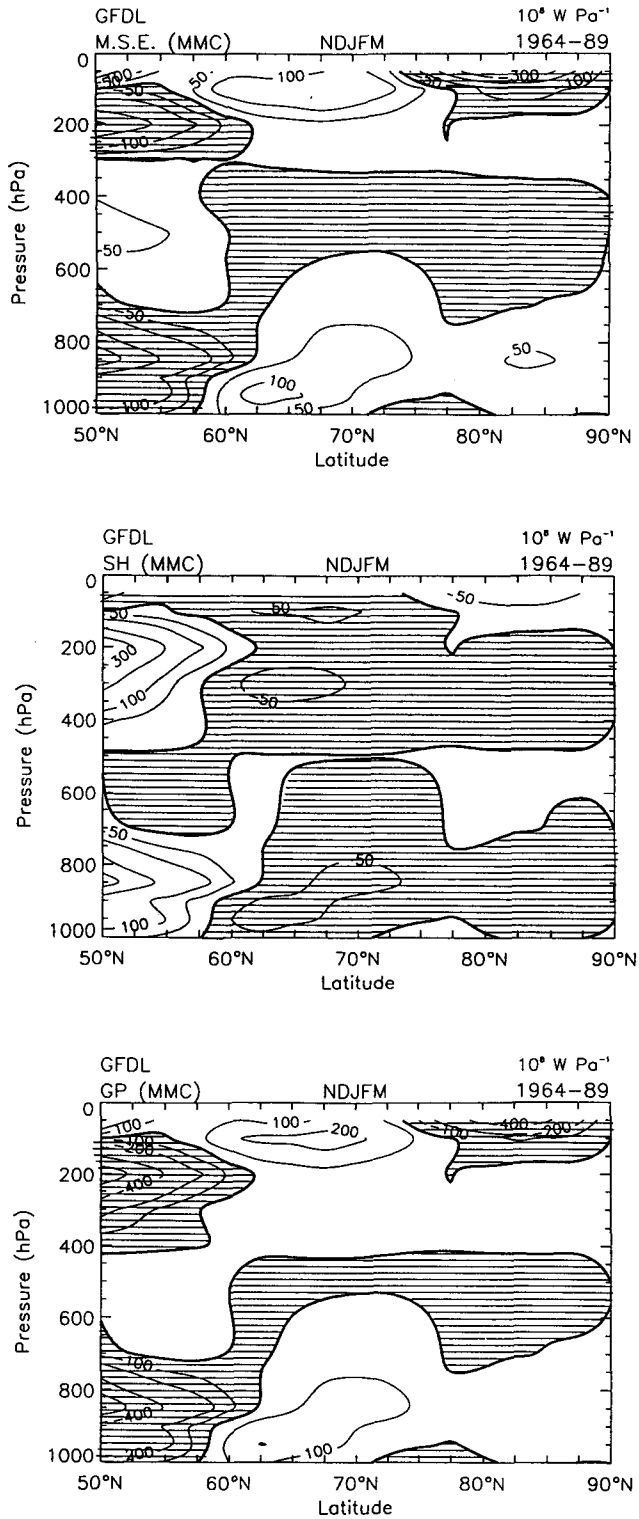


FIG. 3. (a) Poleward flux of moist static energy by the mean meridional circulation in pressure–latitude cross section. Southward flux is shown hatched. Mass-weighted flux contour values are $10^8$ W $Pa^{-1}$. (b) MMC flux of sensible heat in a pressure–latitude cross section, as in Fig. 3a. (c) MMC flux of geopotential energy in a pressure–latitude cross section, as in Fig. 3a.

physical Fluid Dynamics Laboratory flux dataset beyond the 70°N latitude circle. The purpose of this paper is to qualitatively describe the latitudinal variation of the mean meridional circulation north of 50°N and the latitudinal and longitudinal structure of the energy flux convergence over the Arctic basin.

## 2. Techniques

The GFDL dataset of monthly mean variables and flux terms is based on a rawinsonde data at 11 levels from 1000 to 50 mb. The station coverage at 500 mb for the Northern Hemisphere poleward of 55°N is shown in Fig. 1 for a typical month early (January 1969) and later (January 1989) in the period of record (November 1964–August 1989); lack of stations is an issue for the analyses north of 75°N in the western Arctic from 160°E to 130°W and north of 80°N in the remaining Arctic. Several error checks were performed; data beyond plus or minus four standard deviations from the mean for each level and season are excluded. Horizontal fields are developed at each level by objective analyses techniques applied on a 2.5° latitude by 5° longitude grid. Zonal averages of the monthly station values are used as first guess fields (Oort 1983, updated). Only grid points above topography contribute to the statistical field. From inspection of Fig. 1 we have confidence of the quantitative features in the analyzed fields from 60°N to 75°N and to 80°N in the sector from 110°E to 120°W. Lau and Oort (1981) compared the fields generated from the GFDL dataset with those of the National Meteorological Center operational analyses. The GFDL analyses had relatively weaker winds and suppressed the variability over the midlatitude oceans but they had probably more realistic ageostrophic mean meridional circulations. We note the good coverage of land stations at 70°N.

The energy flux into the Arctic across a latitude circle can be expressed as

$$F_{\text{wall}} = \underbrace{\iint Cp[\overline{vT}]\frac{dxdp}{g}}_{\text{MSE}} + \underbrace{\iint g[\overline{vz}]\frac{dxdp}{g}}_{\text{SH}} + \underbrace{\iint L[\overline{vq}]\frac{dxdp}{g}}_{\text{LH}}, \quad (1)$$

where the operator

$$[A] = \frac{1}{2\pi}\int_0^{2\pi} A d\lambda$$

indicates a zonal mean and

$$\bar{A} = \int_0^{\tau} A dt \Big/ \tau$$

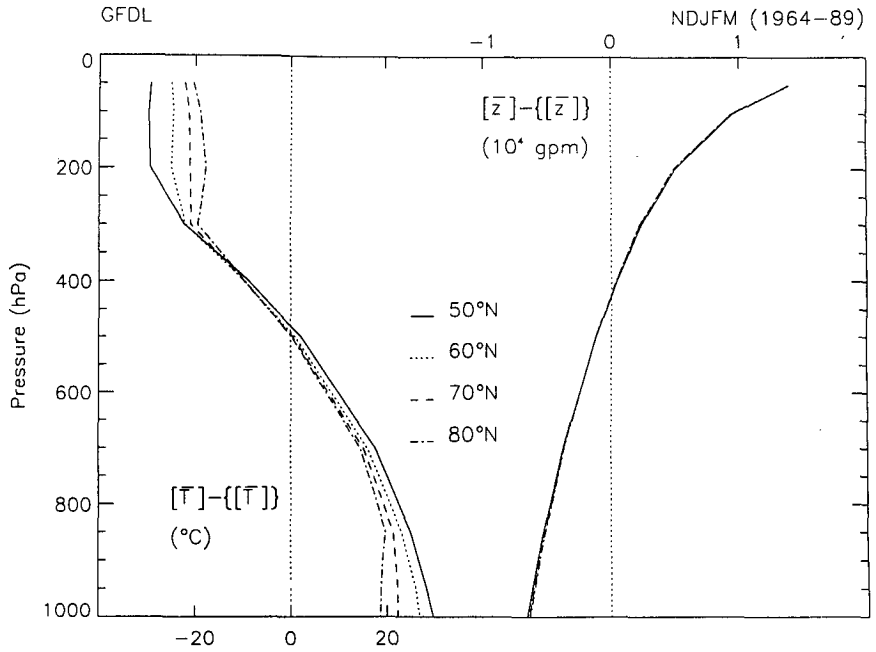


FIG. 3. (*Continued*) (d) Zonal-mean profiles of $T$ and $Z$ with the vertically mass-weighted means removed for four latitude circles, as in Fig. 2b. Scales are on the bottom (°C) for $T$ and on the top ($10^4$ gpm) for $Z$.

indicates a time mean, and $v$ is the northward wind component. Other terms are defined in Table 1. The terms on the right-hand side of (1) are the fluxes of sensible heat (SH), potential energy (GP), and latent heat (LH), collectively termed MSE. Each term in (1) can be expanded into four components: the transient eddy flux (TE), the stationary eddy flux (SE), the mean meridional circulation flux (MMC), and the net mass flow (NMF). For example,

$$\{[\overline{vT}]\} = \underbrace{\{[\overline{v'T'}]\}}_{\text{TE}} + \underbrace{\{[\overline{v}^*\overline{T}^*]\}}_{\text{SE}} + \underbrace{\{[\overline{v}]''[\overline{T}]''\}}_{\text{MMC}} + \underbrace{\{[\overline{v}]\}\{[\overline{T}]\}}_{\text{NMF}}, \quad (2)$$

where

$A' \equiv A - \bar{A}$ departure from time mean
$A^* \equiv A - [A]$ departure from zonal mean
$\{A\} \equiv \int dp/g$ mass-weighted vertical average
$A'' \equiv A - \{A\}$ departure from vertical average.

For monthly time averages we assume that $\{[\overline{v}]\} \approx 0$. This physical constraint is usually not obeyed exactly when using real data. Therefore, we subtract the computed $\{[\overline{v}]\}$ from the vertical profile of the original $[\overline{v}]$ data. Here $\{[\overline{v}]\}$ was $-0.06$ m s$^{-1}$ at 55°N and $+0.03$ m s$^{-1}$ at 70°N. In OT we found difficulties with the value of the 50-mb wind and have replaced the individual monthly values of $[\overline{v}]$ at 50 mb with their 25-year monthly mean value. This replacement influenced the variance but not the means of the computed fluxes. A summary of the fluxes across 70°N is presented in Table 2.

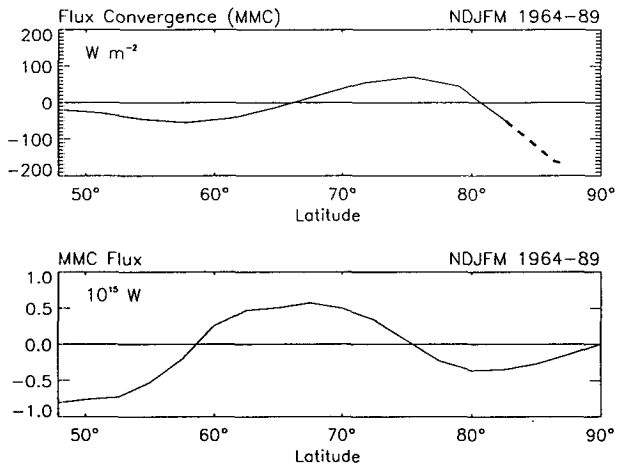


FIG. 4. (a) Latitudinal profile of the flux convergence due to the MMC for winter (NDJFM) based on 25-year averages. Large divergence (cooling) in the winter is based on few or no observations north of 80°N latitude. (b) Same as (a) except for total energy flux by the MMC. The questionable negative values north of 80°N are due to the contribution by the wind component of the MMC at 50 mb.

## 3. Mean meridional circulation

In Fig. 2a the meridional velocity is plotted as a function of pressure for four latitudes for the 5-month win-

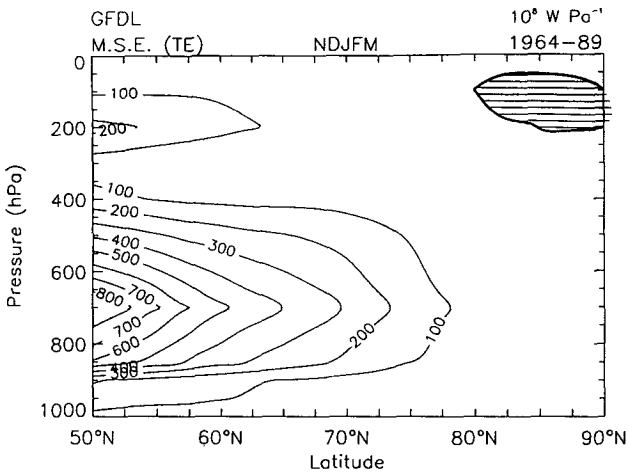


FIG. 5. Pressure–latitude cross section of the zonal-average poleward flux of MSE by transient eddies.

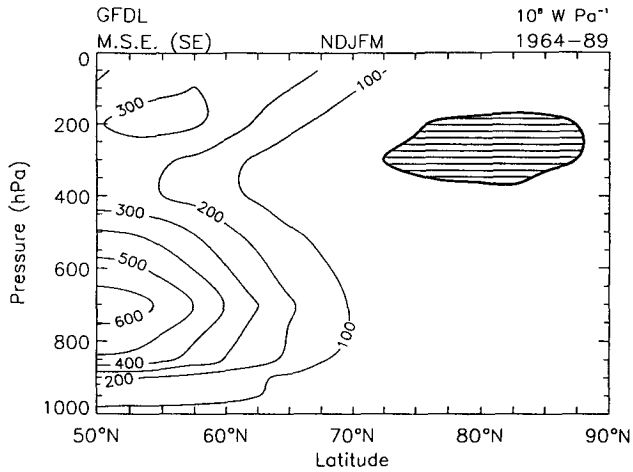


FIG. 6. Pressure–latitude cross section of the zonal-average poleward flux of MSE by stationary eddies.

ter period NDJFM averaged over the 25 years of the GFDL dataset. Figure 2b shows the pressure–latitudinal cross section of the meridional velocity for winter. At 50°N we see the relatively strong Ferrel cell with northward velocities below 700 mb and southward transport up to 100 mb. North of 60°N the flow is reversed with a plausible thermally direct circulation. The circulation peaks near 70°N and again at higher latitudes, although the maximum north of 85° is uncertain based on data density and because (1) is difficult to apply around such a small latitude circle.

Figure 3a shows the moist static energy flux associated with the MMC. We note that the MMC flux of SH is southward (Fig. 3b) at 70°N while that of GP is northward and larger (Fig. 3c). A large southward flux is shown north of 80°N at the 50-mb level in the geo-

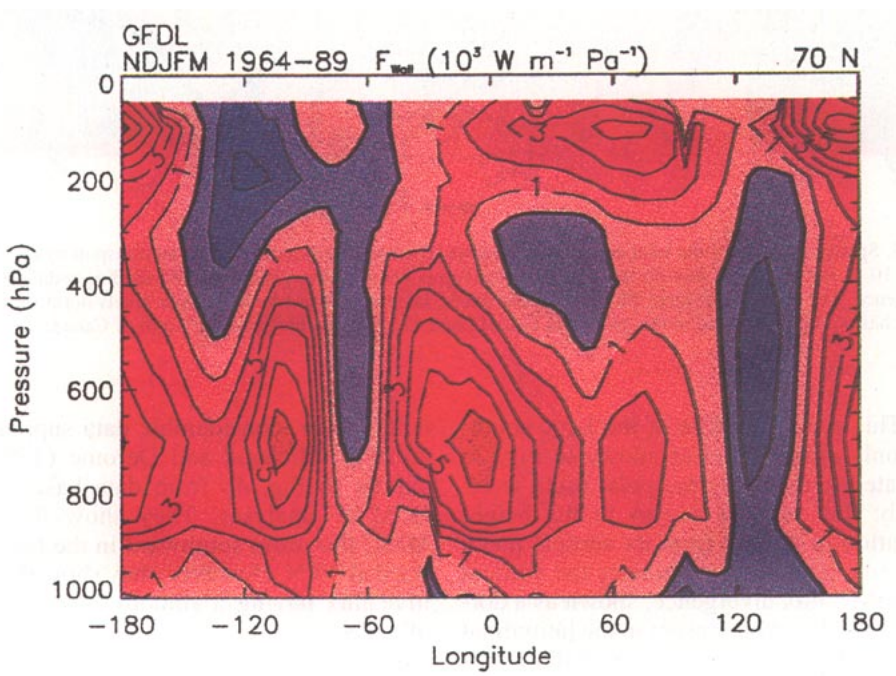


FIG. 7. Longitudinal and vertical variation of the total energy flux across 70°N ($F_{WALL}$). Major northward (red) components are near 0° longitude (Greenland Sea), 110°W (north–central Canada), and 180° (Bering Strait), with a smaller center of poleward flux at 70°E (Kara Sea sector). The only major equatorward flux is at 130°E over Siberia.

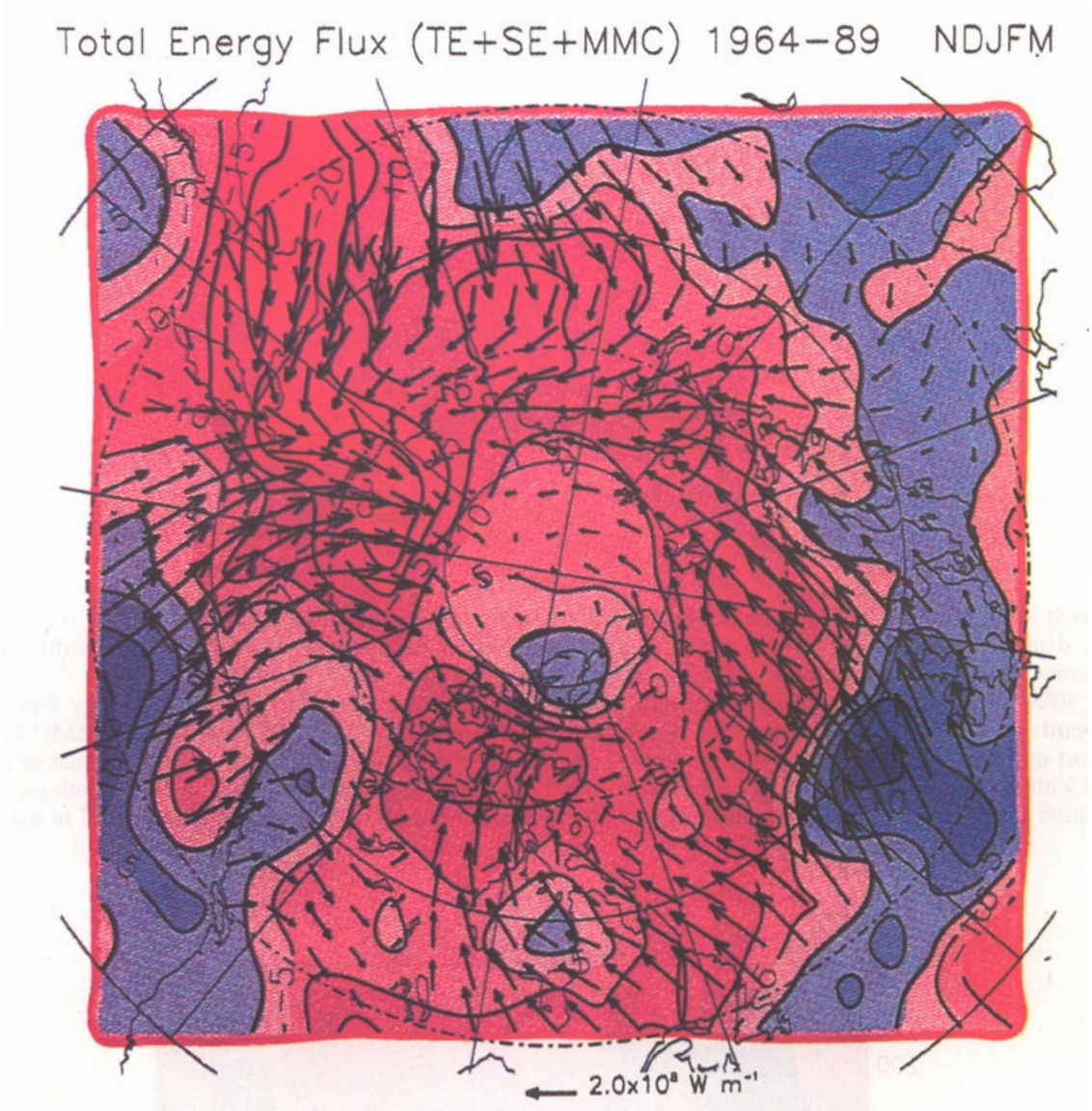


FIG. 8. Spatial variation of the total energy flux. Arrows represent the flux of MSE by all transport modes. Contour lines of 10 W $m^{-2}$ represent flux divergence. Blue shading is net flux divergence, and red shading indicates net flux convergence. The presence of large flux divergence due to large southward flow at upper levels north of 80°N (see Fig. 2a) has not been included in this plot or in Figs. 11 and 12. Note the blue shading north of Canada.

potential flux. This occurs because of the large southward velocity only at this level as shown in Fig. 2a and may be related to resolving the polar night westerlies at 50 mb; this velocity occurs at the height where the deviation in the GP from its vertical mean is largest (Fig. 3d). This level dominates the vertical average of the MMC flux divergence, shown as a dotted line in Fig. 4a, and is even present in the latitudinal fluxes themselves (Fig. 4b). Inspection of the winds at 50 mb shows a gyre that is displaced along the 0° meridian from the pole. The reliability of this component is unknown; there is little direct observational basis for it at this latitude in the original dataset. There is, however, considerable data support for the fluxes at 70°N. Michaud and Derome (1991) show a plot similar to Fig. 4b from data based on six years of ECMWF analyses. They show the reversal in the MMC flux from southward in the Ferrel cell to northward at 70°N. However, they show the northward positive flux having a smooth asymptote to zero north of 80°N.

For comparison we also show the zonal average of the northward transport of SH by transient eddies (Fig. 5) and standing eddies (Fig. 6). Sensible heat represents 86% of the flux by transient eddies at 70°N and 94% of the flux by standing eddies (Table 2). Along

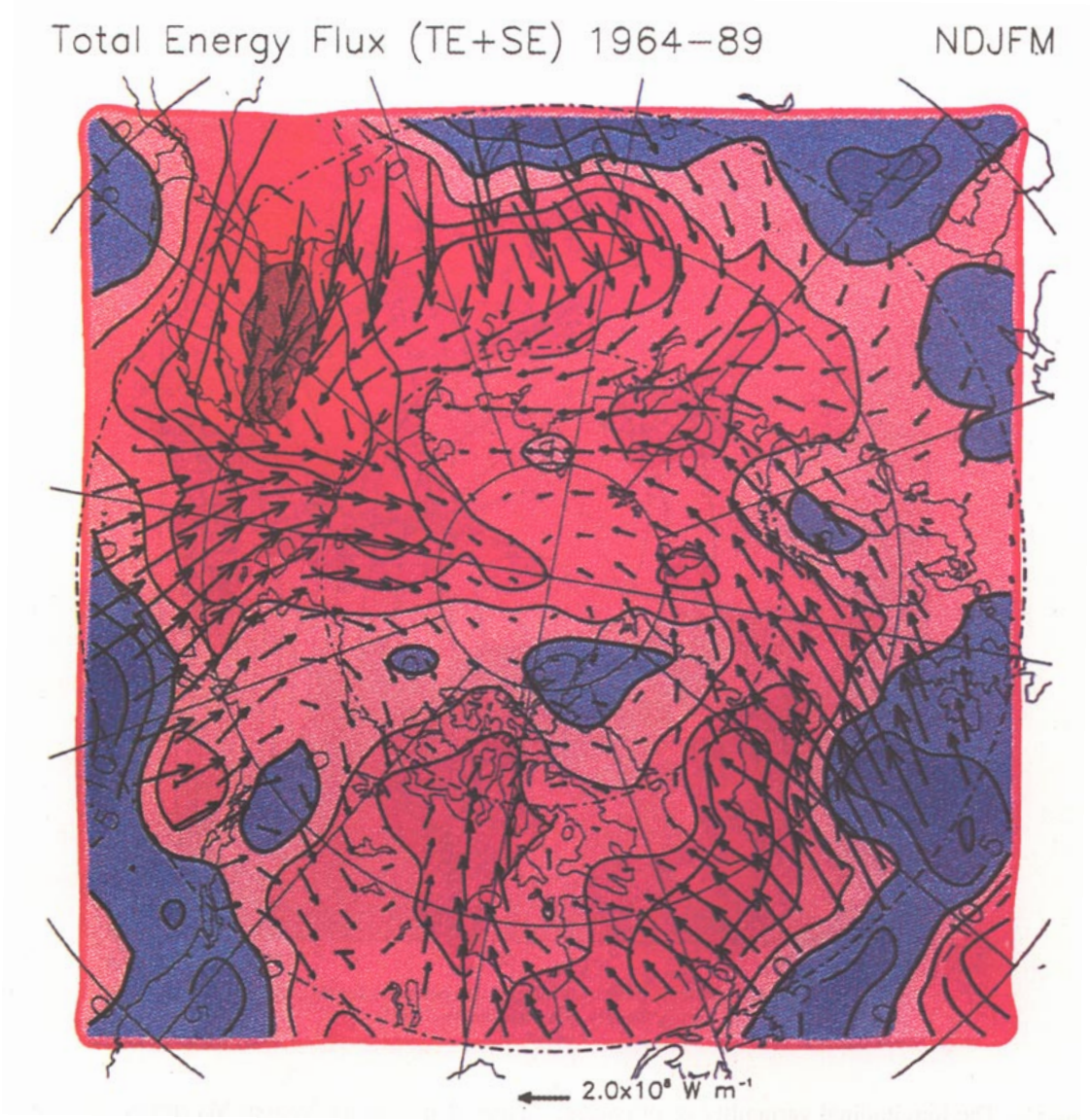


FIG. 9. Same as in Fig. 8 except for showing energy flux by only the standing plus transient eddies.

with the MMC transports of SH and GP, they are the four largest contributors to the latitudinal MSE flux in the Arctic (Table 2).

## 4. Regional variation of flux divergence

The total poleward energy flux across 70°N in a vertical cross section is shown in Fig. 7 (after OT). There are three general pathways: 1) through the Greenland Sea near 0°, 2) east of Siberia/Bering Strait near 180°, and 3) over northern Canada near 100°W. There is evidence of a weak equatorial flux of energy near 130°E.

The pattern in Fig. 7 becomes more coherent when we look at the spatial variations of the total energy flux (Fig. 8). Arrows represent the fluxes, and color shading represents flux convergence with contours of 10 W $m^{-2}$. In computing Fig. 8 we have set the MMC flux convergence to zero north of 81°N (Fig. 4) based on its uncertainty; thus, the values of flux convergence north of 81°N could be considered maximum values. It is also unclear how much influence, if any, a flux divergence at 50 mb would have on the snow surface radiation balance. Figure 9 shows the flux and flux convergence from only the transient and standing eddy components. Comparing Figs. 8 and 9, we note the influence of the Ferrel cell of the MMC decreases the flux convergence south of 60°N and the increased flux convergence from the MMC near 70°N. Other authors, Keith (1995) for example, show an implied flux convergence near 70°N based on ECMWF and NMC grid-

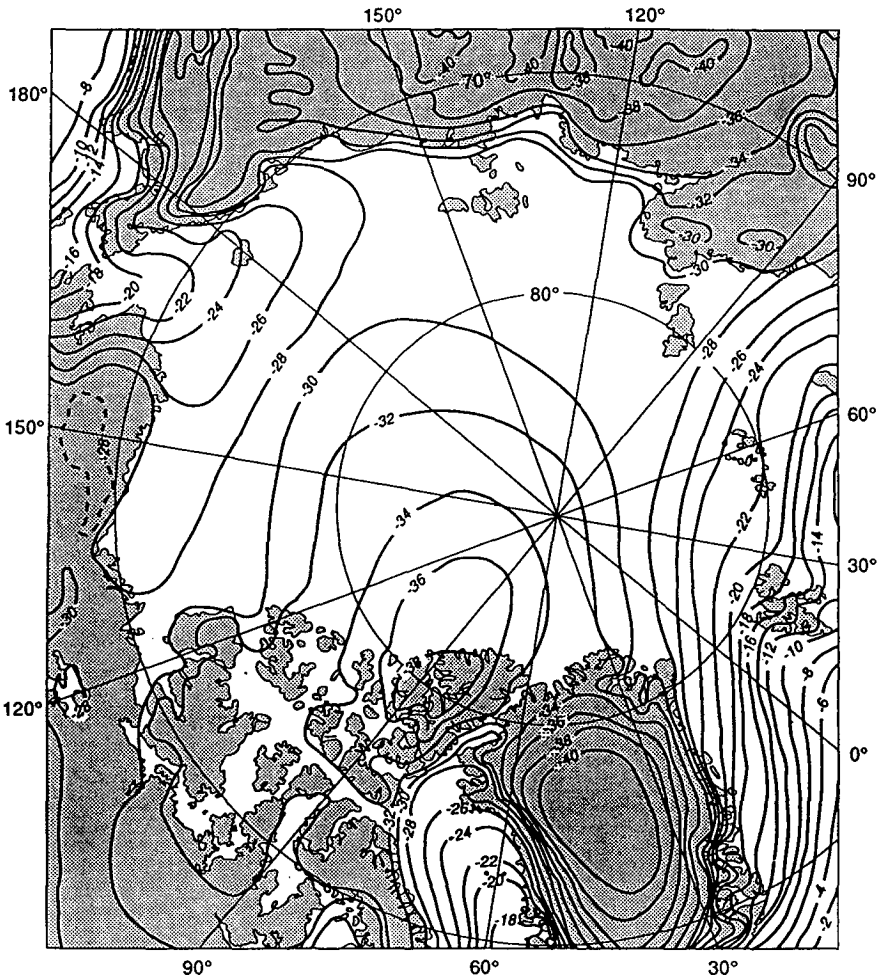


FIG. 10. Climatological mean surface air temperatures for the Arctic during January (after Treshnikov 1985).

ded datasets. The longitudinal variability is, of course, contributed by the eddy fluxes. We see the major regions of flux convergence (red) over Siberia and over the Greenland Sea. The main fluxes into the Arctic relate to the pathway through the Greenland and Barents Seas. The Siberian sector is composed of southward transport of negative deviations of MSE. There are only weak vertical variations of the pattern of flux and flux divergence of MSE (not shown), as suggested by Figs. 5 and 6.

The small center of flux divergence north of Canada in Figs. 8 and 9 is an interesting feature: It implies that there is no, or only weak, compensation by the horizontal flux convergence to balance longwave radiation to space. Based on Figs. 1, 8, and 9 we conclude that the flux convergence is about 50 W $m^{-2}$ less in the Canadian Basin/northern Beaufort Sea region than over the Siberian Arctic/Barents Sea regions. Thus, we would expect colder temperatures and thicker ice in this region. M. Jefferies (1993, personal communication) notes that Sensory System Microwave/Imager (SSM/I) sensors show colder temperatures in this region than over the rest of the Arctic basin. This is also shown in the Gloersen et al. (1992) atlas. The winter flux convergence (Fig. 8) has the same spatial pattern as climatological January surface temperatures (Fig. 10) derived from a large set of Soviet data (Treshnikov 1985), although this cold region is not present in every January (Comiso 1994).

Figure 11 shows the difference in flux convergence for the five years when the energy flux across 70°N was a maximum minus the convergence field for the five years when the flux was a minimum. The main areas of interannual variability are in the Greenland/Barents Sea and eastern Siberian Arctic, the two regions with the largest flux convergence.

Figure 12 shows the flux and flux divergence for the three-month summer period (JJA). The pattern is much smoother than the winter pattern, which is indicative of a much smaller contribution from SE in summer com-

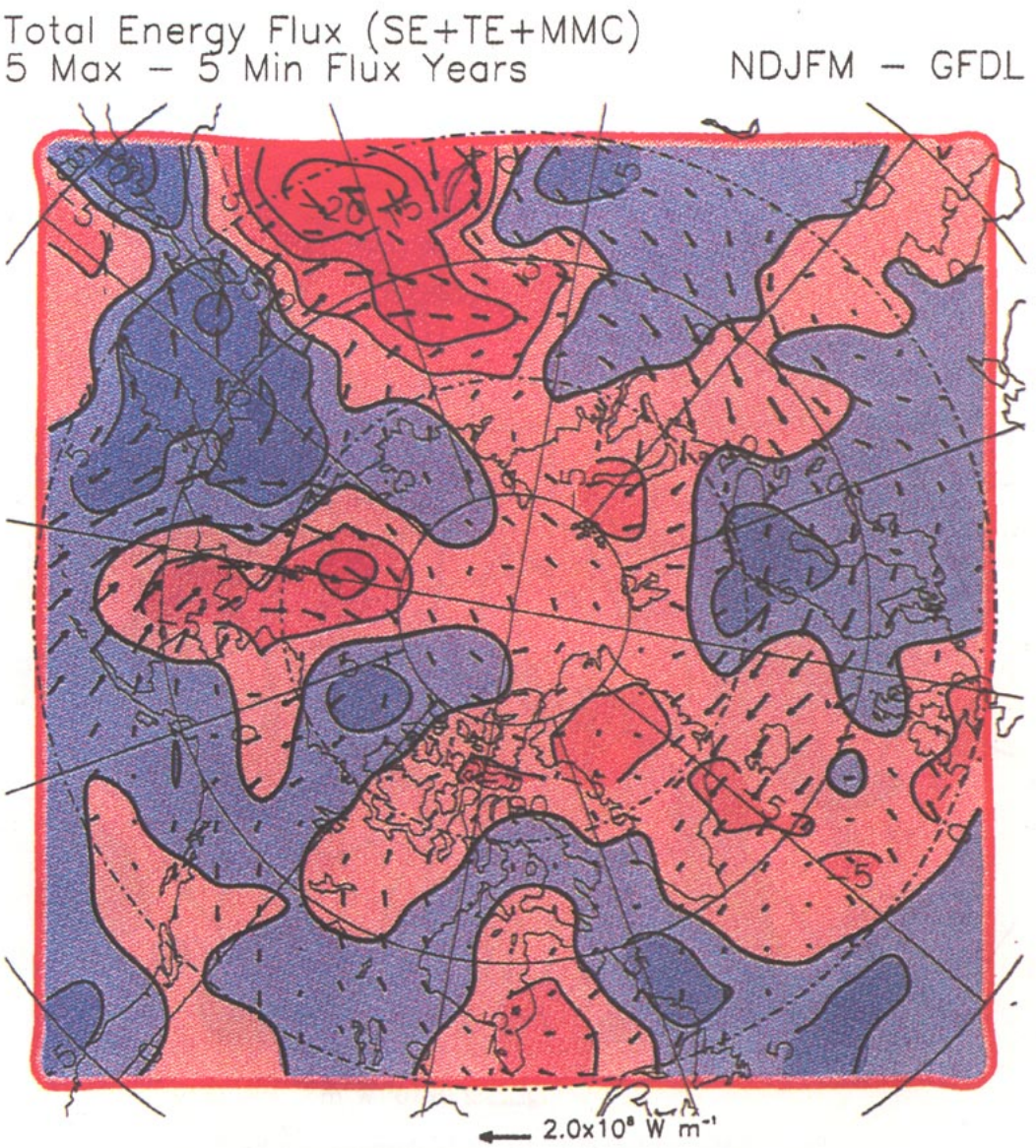


FIG. 11. Flux (arrows) and flux divergence (isolines) of total energy (MSE) for the average of the 5 years out of 25 that had maximum flux ($F_{WALL}$) through 70°N minus the flux and flux divergence for the 5 minimum years. Main areas of convergence are over the Greenland Sea and northeast of Siberia.

pared to winter (Table 2). This result was also seen by Michaud and Derome (1991) and Kann et al. (1994). A pressure latitudinal cross section for JJA of MSE is shown in Fig. 13.

Other authors have investigated the energy fluxes into higher latitudes using operational gridded analyses. Higuchi et al. (1991) looked at the spatial and temporal patterns of the TE transport of sensible heat using an average of 500-mb and 1000-mb geostrophic winds. Carleton (1988) and Rogers and Raphael (1992) looked at the TE and SE transport of sensible heat on the 700-mb level. All of these authors noted similar spatial patterns of fluxes, as in Fig. 9, with centers over the Barents Sea with northward transport of positive anomalies, and a correlation of southward transport of negative anomalies in the east Siberia sector. Carleton noted increased poleward flux with the Greenland below mode (stronger Icelantic low) of the North Atlantic Oscillation (NAO). Higuchi et al. (1991) showed a correlation between the northward sensible heat flux and the minimum Greenland Sea ice extent. Rogers and Raphael (1992) showed larger standing eddies in the northern Siberian sector with a positive Pacific North American (PNA) oscillation. Our results compare with Serreze and Barry (1988) in that a major pathway for energy flux into the Arctic is associated with storm

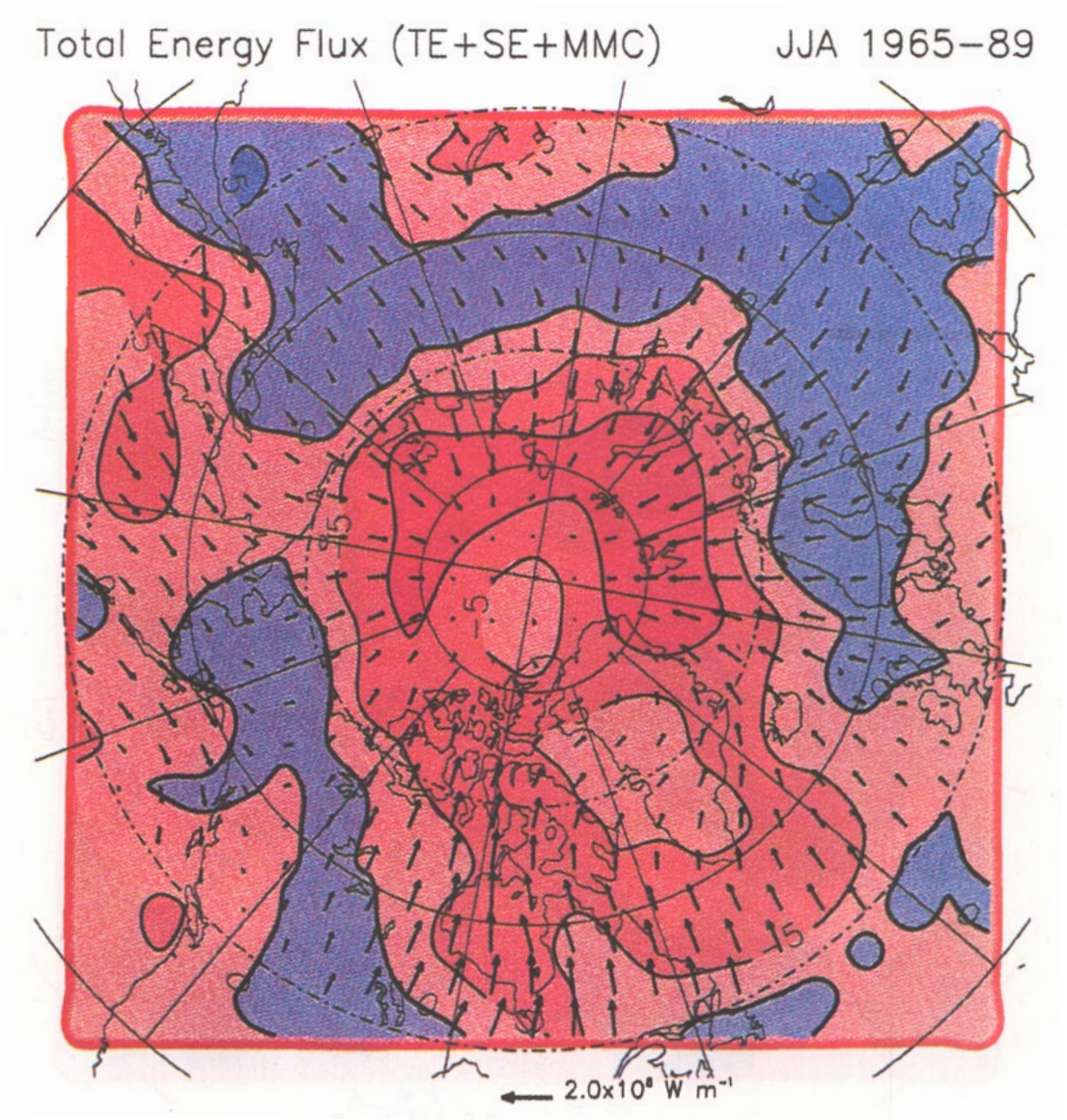


FIG. 12. Spatial variations of the flux and flux divergence, as in Fig. 8, for summer (JJA) for a 25-year average (1965–1989).

tracks through the Atlantic sector. We differ with Higuchi et al. (1991) in that, although the energy flux in the Siberian sector is important, it does not represent a region of large interannual variability; our Fig. 11 shows that this sector does contribute to the interannual variability of the flux across 70°N. The interannual variability in both the Greenland Sea and the east Siberian sectors is mainly due to the variability in the strength of the standing eddy field.

## 5. Conclusions

Based on 25 years of the GFDL dataset we have evaluated the mean meridional circulations and flux convergence of moist static energy north of 55°N. The mean meridional circulation changes from the Ferrel cell south of 60°N to a thermally direct cell centered near 70°N. The data density based on the number of land stations at this latitude provides confidence in these results. A large and uncertain meridional velocity at 50 mb north of 80°N suggests a difficulty in closing the MMC circulation at this latitude. Indeed, the concept of a zonal mean breaks down over such small areas. Because the MMC is zonally symmetric, this difficulty does not influence the conclusion that the flux convergence is different in the western versus the eastern Arctic.

Much of the flux convergence from the MMC occurs over land or at the periphery of the central Arctic basin. The main poleward TE and SE fluxes occur in the

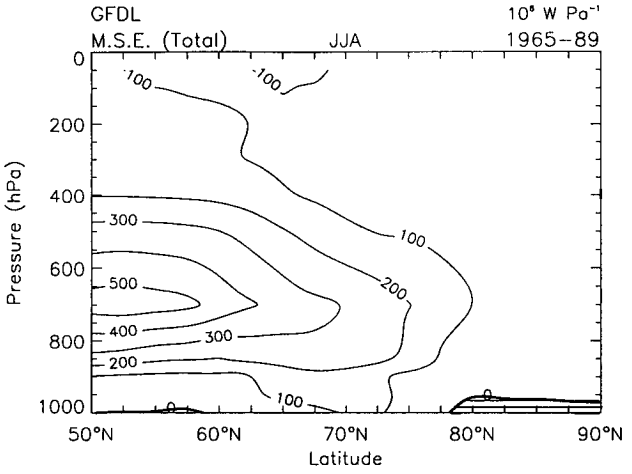


FIG. 13. Pressure–latitude cross section of the zonal-average poleward flux of MSE by all transport components.

Greenland/Barents Sea and eastern Siberia. The maximum change in flux convergence for the five maximum minus the five minimum winters for heat flux across 70°N also occurs in these two sectors. There is a minimum in flux convergence north of Canada in the western Arctic. The spatial pattern of atmospheric flux convergence of moist static energy for the Arctic is nearly identical to the distribution of January surface air temperatures, which suggests a strong radiative tie between the snow surface and the atmospheric temperatures in the air column above (Overland and Guest 1991).

*Acknowledgments.* Preparation of this paper was supported in part by Arctic Programs, Office of Naval Research and the Polar Research Program, NASA. We thank Paul Quicker and Ryan Whitney for preparation of the manuscript.

## REFERENCES

Carleton, A. M., 1988: Meridional transport of eddy sensible heat in winters marked by extremes of the North Atlantic Oscillation, 1948/49–1979/80. *J. Climate,* **1,** 212–223.

Comiso, J. C., 1994: Surface temperatures in the polar regions from Nimbus 7 temperature humidity infrared radiometer. *J. Geophys. Res.,* **99,** 5181–5200.

Gloersen, P., W. J. Campbell, D. J. Cavalieri, J. C. Comiso, C. L. Parkinson, and H. J. Zwally, 1992: *Arctic and Antarctic Sea Ice 1978–1987: Satellite Passive-Microwave Observations and Analysis.* NASA, 290 pp.

Higuchi, K., C. A. Lin, A. Shabbar, and J. L. Knox, 1991: Interannual variability of the January tropospheric meridional eddy sensible heat transport in northern latitudes. *J. Meteor. Soc. Japan,* **69,** 459–472.

Kann, D. M., S. Yang, and A. J. Miller, 1994: Mean meridional transport of energy in the earth–atmosphere system using NMC global analyses and ERBE radiation data. *Tellus,* **46A,** 553–565.

Keith, D. W., 1995: Meridional energy transport: uncertainty in zonal means. *Tellus,* **47A,** 30–44.

Lau, N., and A. H. Oort, 1981: A comparative study of observed northern hemisphere circulation statistics based on GFDL and NMC analyses. Part I: The time-mean fields. *Mon. Wea. Rev.,* **109,** 1380–1403.

Michaud, R., and J. Derome, 1991: On the mean meridional transport of energy in the atmosphere and oceans as derived from six years of ECMWF analyses. *Tellus,* **43A,** 1–14.

Maykut, G. A., 1986: The surface heat and mass balance. *The Geophysics of Sea Ice,* NATO ASI Ser. B., Vol. 146, N. Untersteiner, Ed., 395–464.

Moritz, R. E., J. A. Beesley, and K. Runciman-Moore, 1992: Modeling the interactions of sea ice and climate in the central arctic. *Third Conf. Polar Meteorology and Oceanography,* Portland, OR, Amer. Meteor. Soc., 105–108.

Nakamura, N., and A. H. Oort, 1988: Atmospheric heat budgets of the polar regions. *J. Geophys. Res.,* **93,** 9510–9524.

Oort, A. H., 1983: Global atmospheric circulation statistics, 1958–1973. NOAA Prof. Paper 14, 180 pp. (Available from the author.)

Overland, J. E., and P. S. Guest, 1991: The Arctic snow and air temperature budget over sea ice during winter. *J. Geophys. Res.,* **96,** 4651–4662.

——, and P. Turet, 1994: Variability of the Atmospheric Energy Flux across 70°N computed from the GFDL data set. *Nansen Centennial Volume, Geophys. Monogr.,* **84,** Amer. Geophys. Union, 313–325.

Rogers, J. C., and M. N. Raphael, 1992: Meridional eddy sensible heat fluxes in the extremes of the Pacific/North American teleconnection pattern. *J. Climate,* **5,** 127–139.

Royer, J. F., S. Planton, and M. Deque, 1990: A sensitivity experiment for the removal of Arctic sea ice with the French spectral circulation model. *Climate Dyn.,* **5,** 1–17.

Serreze, M. C., and R. G. Barry, 1988: Synoptic activity in the Arctic basin, 1979–85. *J. Climate,* **1,** 1276–1295.

Thorndike, A. S., 1992: A toy model linking atmospheric thermal radiation and sea ice growth. *J. Geophys. Res.,* **97,** 9401–9410.

Treshnikov, A. F., 1985: *Atlas of the Arctic.* Arctic and Antarctic Institute, 204 pp.

Untersteiner, N., 1990: Some problems of sea ice and climate modeling. *Veröffentlichungen der Universität Innsbruck,* Heraus Geber, 209–228.